



Delft University of Technology

Gradient Origami Metamaterials for Programming Out-of-Plane Curvatures

Hedayati, Reza; Roudbarian, Nima; Tahmasiyan, Sara; Bodaghi, Mahdi

DOI

[10.1002/adem.202201838](https://doi.org/10.1002/adem.202201838)

Publication date

2023

Document Version

Final published version

Published in

Advanced Engineering Materials

Citation (APA)

Hedayati, R., Roudbarian, N., Tahmasiyan, S., & Bodaghi, M. (2023). Gradient Origami Metamaterials for Programming Out-of-Plane Curvatures. *Advanced Engineering Materials*, 25(14), Article 2201838. <https://doi.org/10.1002/adem.202201838>

Important note

To cite this publication, please use the final published version (if applicable). Please check the document version above.

Copyright

Other than for strictly personal use, it is not permitted to download, forward or distribute the text or part of it, without the consent of the author(s) and/or copyright holder(s), unless the work is under an open content license such as Creative Commons.

Takedown policy

Please contact us and provide details if you believe this document breaches copyrights. We will remove access to the work immediately and investigate your claim.



Spray Coating Experiments: Setups and Methodologies



**The latest eBook from
Advanced Optical Metrology.
Download for free.**

Spray Coating Experiments: Setups and Methodologies, is the third in our Thin Films eBook series. This publication provides an introduction to spray coating, three article digests from Wiley Online Library and the latest news about Evident's Image of the Year Award 2022.

Wiley in collaboration with Evident, are committed to bridging the gap between fundamental research and industrial applications in the field of optical metrology. We strive to do this by collecting and organizing existing information, making it more accessible and useful for researchers and practitioners alike.

EVIDENT
OLYMPUS

WILEY

Gradient Origami Metamaterials for Programming Out-of-Plane Curvatures

Reza Hedayati,* Nima Roudbarian, Sara Tahmasiyan, and Mahdi Bodaghi*

Origami structures are a traditional Japanese art that have recently found their way into engineering applications due to their powerful capability to transform flat 2D structures into complex 3D structures along their creases. This has given a rise to their application as designer materials with unprecedented mechanical characteristics, also known as metamaterials. Herein, gradient Miura-ori origami metamaterials are introduced as a method to preprogram out-of-plane curvatures. Several types of unit cell distributions in the origami lattice structure including checkered, linear gradient, concave radial gradient, convex radial gradient, and striped are considered. The results show that these distributions of Miura-ori origami can create single- or double curvatures including twisting, saddling, bending, local inflation, local twisting, local bending, and wavy shapes, when the origami metamaterial is loaded in compression. All the Gaussian curvatures (negative, positive, and zero) can be achieved using the proposed models. The approach helps tailoring complex preprogrammed surface geometries by employing linearly varying gradient distributions of Miura-ori origami.

structures are a traditional Japanese art, which have recently found their way into metamaterials research due to their powerful capability to transform flat 2D structures into complex 3D structures along their creases.^[7] Particularly, Miura-ori origami, also known as herringbone geometry (Figure 1a,b), has been proposed as an origami-based mechanical metamaterial.^[8] This design was first invented to pack solar panels efficiently, but it is relevant to note that this pattern also occurs in natural structures such as leaves, embryonic intestines,^[9] and vertebrate guts.^[10] The mathematical richness and tunability of Miura-ori geometry allow using it in different scales from the nanometric level to architecture.^[11] The suitability of Miura-ori for engineering applications lies in its four spectacular characteristics: being able to be folded rigidly, having only one

degree of freedom, having negative Poisson's ratio, and being flat-foldable.^[11]

3D exotic materials with negative Poisson's ratio (known as auxetics metamaterials) offer extreme mechanical properties such as high shear resistance, energy absorption, indentation resistance, and toughness.^[12] When used in 2D setting, a structure with spatially incompatible auxetic properties can create various 3D shapes through out-of-plane buckling.^[13]

Given the richness of the Miura-ori origami, the question that arises here is whether or not it is possible to create basic well-known Euclidean and non-Euclidean 3D curvatures using Miura-ori metamaterials upon application of an external stimulus such as mechanical load. There have been a few studies that have used origami tessellations to create preprogrammed (not necessarily 3D) curvatures.^[8,11,14] In a recent study,^[15] homogenization-type two-scale asymptotic method was suggested to reconstruct arbitrary smooth surfaces that can be fitted by a given periodic truss that satisfy a known set of partial differential equations. Two recent studies presented optimization-based method procedures to produce Miura-ori tessellations^[11,16] programmed to create 3D geometries with some approximations. Despite attempts to create Miura-ori tessellations which would lead to desired curvatures with some approximations, no study has been carried out on how linearly varying gradient distributions of Miura-ori unit cells (see Figure 1c) can be used to create various well-known 3D curvatures. Linearly varying Miura-ori distributions (rather than non-uniform ones created by numerical models) have the advantages of being easy to understand and thus easy to implement for practical problems, for example as building blocks for complex actuators.


1. Introduction

Designer materials, where rationally designed geometry at the small scale gives rise to unusual materials properties at the macro-scale, are often called metamaterials.^[1–6] Origami

R. Hedayati
Department of Aerospace Structures and Materials
Faculty of Aerospace Engineering
Delft University of Technology (TU Delft)
Kluyverweg 1, 2629 HS Delft, The Netherlands
E-mail: r.hedayati@tudelft.nl

N. Roudbarian, S. Tahmasiyan
School of Mechanical Engineering
College of Engineering
University of Tehran
Tehran PO Box 515-14395, Iran

M. Bodaghi
Department of Engineering
School of Science and Technology
Nottingham Trent University
Nottingham NG11 8NS, UK
E-mail: mahdi.bodaghi@ntu.ac.uk

 The ORCID identification number(s) for the author(s) of this article can be found under <https://doi.org/10.1002/adem.202201838>.

© 2023 The Authors. Advanced Engineering Materials published by Wiley-VCH GmbH. This is an open access article under the terms of the Creative Commons Attribution License, which permits use, distribution and reproduction in any medium, provided the original work is properly cited.

DOI: 10.1002/adem.202201838

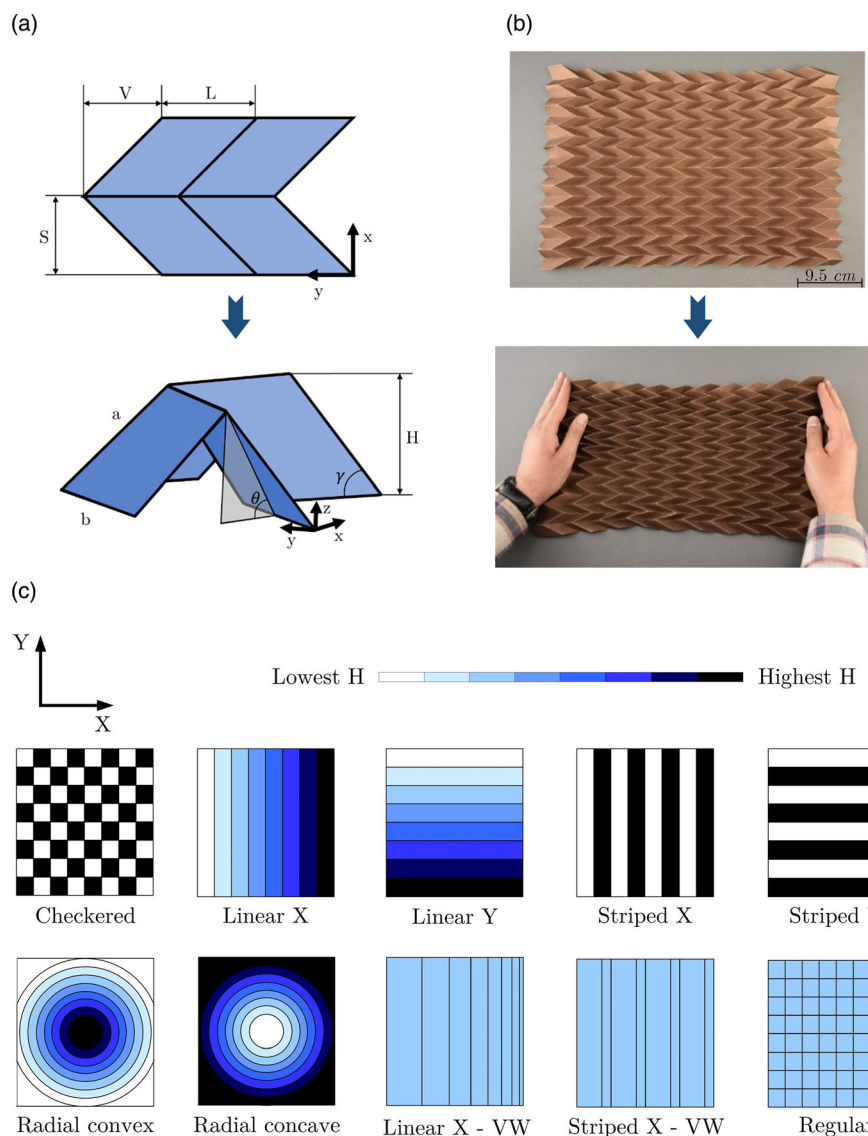


Figure 1. a) Geometry and dimensions of unit cells of a Miura-ori origami structure, b) Miura-ori origami with uniform unit cell distribution before and after compression, c) schematic of variations of mountain heights and widths in different lattice structures consider in this study. The darker the color, the higher the mountain height is.

In this article, for the first time, we introduce basic gradient origami metamaterials as a tool to create programmable 3D curvatures. In our previous work,^[17] we demonstrated how using gradient distributions of re-entrant auxetics can lead to action-at-a-distance actuators. While such block-shaped actuators are useful in many applications such as soft robotics, sensors, and controllers,^[17] curved actuators seem to offer more exciting functionalities useful in more advanced configurations. For this aim, nine unit cell distributions are proposed and analyzed mechanically. The proposed designs are fabricated using kraft papers and are then loaded in compression. A numerical finite element approach is also implemented to evaluate the experimental results, as well as to compare the designs in terms of main mechanical properties.

2. Geometries

We chose the patterns in such a way that we could achieve all the Gaussian curvatures (negative, positive, and zero) as well as several primary deformations known in the actuation field. Since the in-plane longitudinal and lateral sides of each unit cell are constrained by its neighboring unit cells as well as the far-field applied boundary conditions, under compression, the unit cells locally and the origami lattice structure as a whole have to deform in the out-of-plane direction to compensate for the space they require for deformation. It is evident that higher mountain heights in Miura-Ori unit cells lead to higher out-of-plane deformations. We visualized the lateral deformations we expected as a result of longitudinal compression. Afterward, based on the

envisioned deformations (bending, twisting, local inflammation, and saddle-shaped), the unit cell distributions were chosen.

Several types of tessellations with variable mountain height namely checkered, linear gradient (in both the X and Y directions), striped (in both the X and Y directions), concave radial gradient, convex radial gradient, and regular were considered (Figure 1c). It must be noted that the XY plane is the plane parallel to the mid-plane of the origami lattice structure (see Figure 1a,c). In most of the structures, regardless of the mountain peak height, the parameters S , L , and V were set constant and equal to $S = 19.64$ mm, $L = 19.84$ mm, and $V = 22.68$ mm. The overall length of the origami lattice structures in each direction was therefore 392.7 mm. The maximum and minimum heights of the mountains in all the simulated configurations were considered as $H_{\max} = 22.5$ mm and $H_{\min} = 4.5$ mm, respectively. The variation of mountain height in the Linear-X, Linear-Y, Radial-Convex, and Radial-Concave topologies from a cell to the adjacent cell was chosen to be linear. The checkered structure, although not being strictly a flat-foldable geometry, was manufactured from flat papers due to having a configuration which is close to flat-foldable conditions. Some of the above-mentioned geometries, due to including nonflat surfaces, or due to including particular patterns were not possible to be manufactured by folding flat plates. Therefore, to make the origamis foldable from flat papers, in addition to the noted structures, two additional geometries (linear X and striped X) in which instead of mountain height, unit cell width was varied was also considered, denoted by VW (variable width) afterward. In the Linear-X-VW and striped X-VW structures, the mountain height was selected to be 22.4 mm, and the dimension L of cell was increased linearly. The range of changes of L for Linear-X-VW topology was 27.49 – 52.24 mm, and the small and large L for striped X-VW was 23.5 and 55 mm, respectively. The dimensions of Miura-origami are^[18]

$$a = \sqrt{L^2 + H^2} \quad (1)$$

$$\theta = \sin^{-1}\left(\frac{H}{a \sin(\gamma)}\right) \quad (2)$$

$$V = \frac{S}{\cos(\theta) \tan(\gamma)} \quad (3)$$

$$b = V\sqrt{1 + \cos^2(\theta)\tan^2(\gamma)} \quad (4)$$

For the unit cells with maximum height, $\theta = \gamma = \frac{\pi}{3}$ and $a = b = 3$ mm. For the unit cells with minimum height, we set $\gamma = \frac{\pi}{9}$.

3. Methods

The specimens were generated from the original Miura-ori crease pattern. According to 3D models, creases were designed, transferred to papers, and folded by hand. Thin kraft papers with thicknesses of 250 μm were used as initial flat sheets. All the specimens were made in one piece. All the fabricated origamis were placed vertically, and their lower edge was constrained using glue. The top edge of the origami lattices was displaced downward.

ANSYS finite element (FE) modeling package was used to construct the geometry of the origami lattices and to carry out the simulations. An algorithm was developed to vary the unit cell height H or width S (Figure 1a) depending on the type of tessellation. Each crease line was discretized using 10 elements. Therefore, each lattice structure consisted of 40 000 planar elements (SHELL 181 in ANSYS library). The material properties of Kraft paper were given to the models ($E_s = 1.7$ GPa and $\nu = 0.4$). The thickness of the origami was set to 250 μm . One side of each origami tessellation was constrained in the Y direction, and the other side was compressed in the Y direction ($\delta_z = 6$ mm). The other degrees of freedom were kept free to allow out-of-plane displacements. 10×10 tessellations were used for all the computational models.

4. Results

In several tessellations, flat-foldability conditions based on Kawasaki's theorem were met which made them manufacturable by folding (Figure 2). Based on Kawasaki's theorem, a structure is flat-foldable if the sums of even and odd sequence of angles, each, equal to π . The tessellations that did not satisfy the Kawasaki's conditions were only modeled numerically (Figure 3a). Thanks to novel manufacturing technologies, such as Additive Manufacturing, such nonflat-foldable structures are now realizable.^[19] The manufactured origamis namely checkered, linear X-VW, linear Y gradient, striped X-VW, and striped Y provided twisting, local inflammation, saddle, bending, and wavy deformations, respectively (Figure 2).

The numerical results show that structures that departed (slightly or highly) from flat-foldability conditions namely linear X gradient (with variable mountain height), striped X (with variable mountain height), concave radial gradient, and convex radial gradient distributions of unit cells showed, respectively, local twisting, local bending, saddle-shape, and saddle-shape deformations (Figure 3a). Therefore, the results show that different proposed tessellation types have been able to transform their shape into different 3D curvatures by means of in-plane incompatibilities. Overall, the achieved 3D curvatures from the nine proposed tessellations include twisting, local inflammation, saddle-shape, bending, wavy shape, local bending, and local twisting (Figure 2 and 3a).

The maximum out-of-plane displacement to initial axial unit cell length (U_z/L) at $\epsilon_y = 0.01$ of the checkered, linear X-VW gradient, linear Y gradient, striped X-VW, striped Y, linear X gradient, striped X, concave radial gradient, and convex radial gradient structures were 6.6×10^{-3} , 0.73×10^{-3} , 3.2×10^{-3} , 1.6×10^{-3} , 2.3×10^{-3} , 5×10^{-3} , 2.5×10^{-3} , 3.1×10^{-3} , and 3.8×10^{-3} , respectively (Figure 3b). The linear X structure had a relatively high maximum/minimum U_z ratio, and the other geometries demonstrated similar levels of maximum/minimum U_z ratio (Figure 3d). The checkered and linear X-VW gradient had the highest stiffness levels, while the linear X and radial convex gradient patterns had the lowest stiffness values (Figure 3e).

5. Discussions

The underlying physical mechanism governing the deformations of most of the proposed designs relates to the differences in local

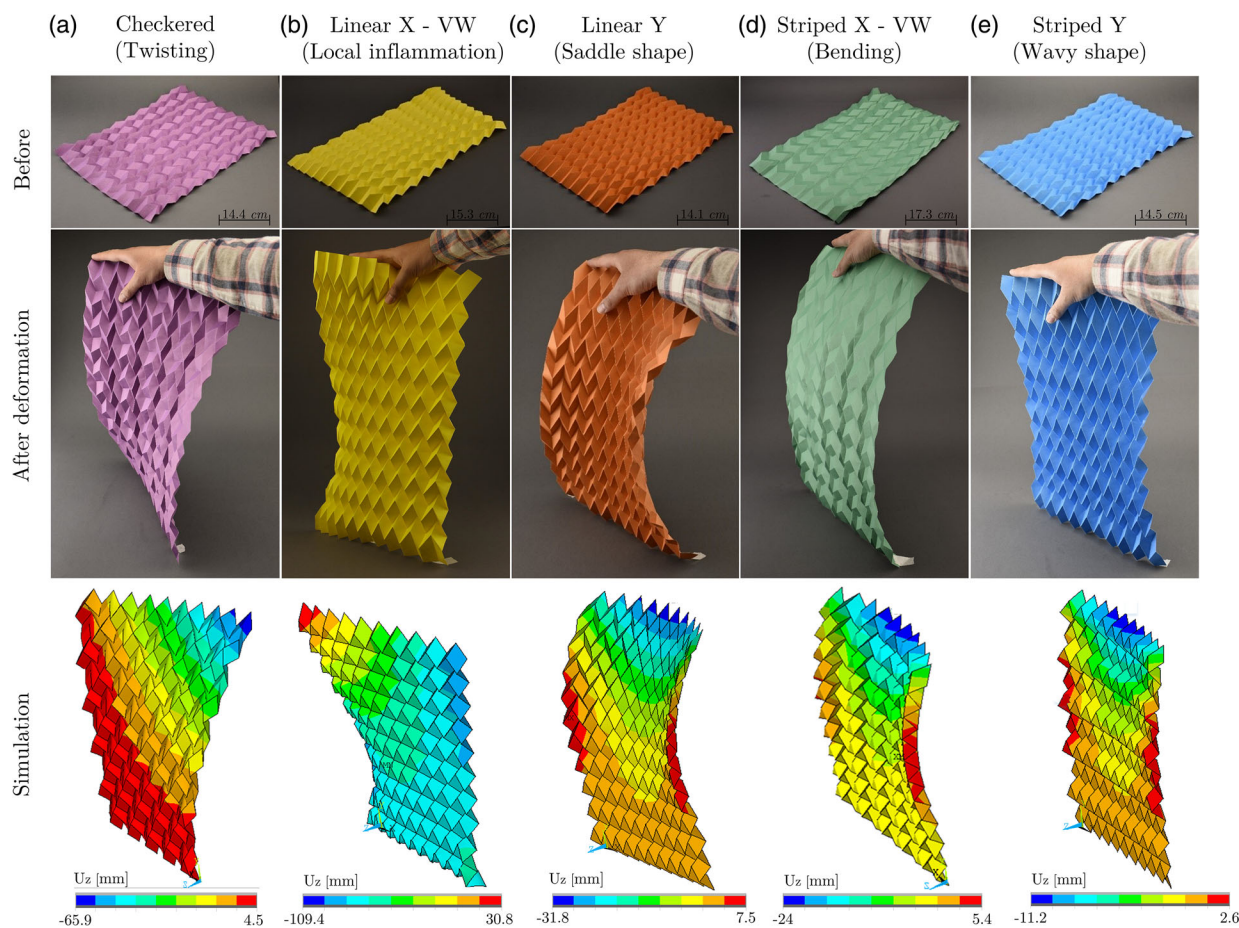


Figure 2. Experimental and numerical deformation of a) checkered, b) linear X–VW gradient, c) linear Y gradient, d) striped X–VW, and e) striped Y tessellations.

axial stiffness of the unit cells. The higher the mountain height in a unit cell is, the smaller the axial stiffness of the unit cell becomes (as bending in the folds occurs with more ease).^[20] Under the same level of external force, the unit cells with lower stiffness levels respond with a higher degree of axial flexibility. However, as all the unit cells possess similar axial space for deformation, the unit cells with lower stiffness compensate for the insufficient axial space with out-of-plane deformations. In other words, the out-of-plane deformation of any part of the gradient lattice structure has a direct relationship with the mountain height at that point. The higher the mountain height in a part of a gradient lattice origami is, the more the observed level of out-of-plane displacements becomes. Therefore, with the proper arrangement of gradient patterns in the origami structure, the desired 3D curvature under axial compression can be obtained.

Unlike the gradient origamis, the nongradient lattice structures each have a distinct underlying deformation mechanism. For instance, the checkered structure shows twisting under compression since that the unit cells with low mountain height on the one hand and the unit cells with high mountain height on the other hand are positioned in a cross configuration. For convenience, only consider a 2×2 portion of the checkered structure. While one diagonal of the considered portion tends to have low

out-of-plane deformation, the other diagonal tends to have high out-of-plane deformation. This would lead to twisting in that portion, and as a result, the whole lattice. In each row of the striped X–VW structure, the stiffness of each pair of neighboring unit cells is identical to the stiffness of their adjacent pairs. Therefore, the tendency to out-of-plane deformation does not cause any curvature along the X direction, while the necessity for more space creates curvature in the YZ plane. In each column of an envisioned striped Y–VL (VL standing for variable length) structure, all the unit cell pairs have the same stiffness, and as a result, similar to the previous case (striped X–VW), no curvature in the Y direction is expected to be observed. The described mechanisms for the deformation of striped Y–VL and striped X–VW are also valid to some degree for the striped Y and striped X lattices, although to a lesser extent, as deviation from flat-foldability causes some complexities in the deformations.

It is well known that flat-foldable origamis that have one degree of freedom are easily deployable and energy efficient. One way of making the nonflat-foldable structures (Figure 3a) flat-foldable is to consider some holes in their structure and thus to transform the Miura-Ori origami structures into Miura-Ori hybrid origami-kirigami structures. Kirigami is a variation of origami that includes cutting in the sheet in addition to foldable

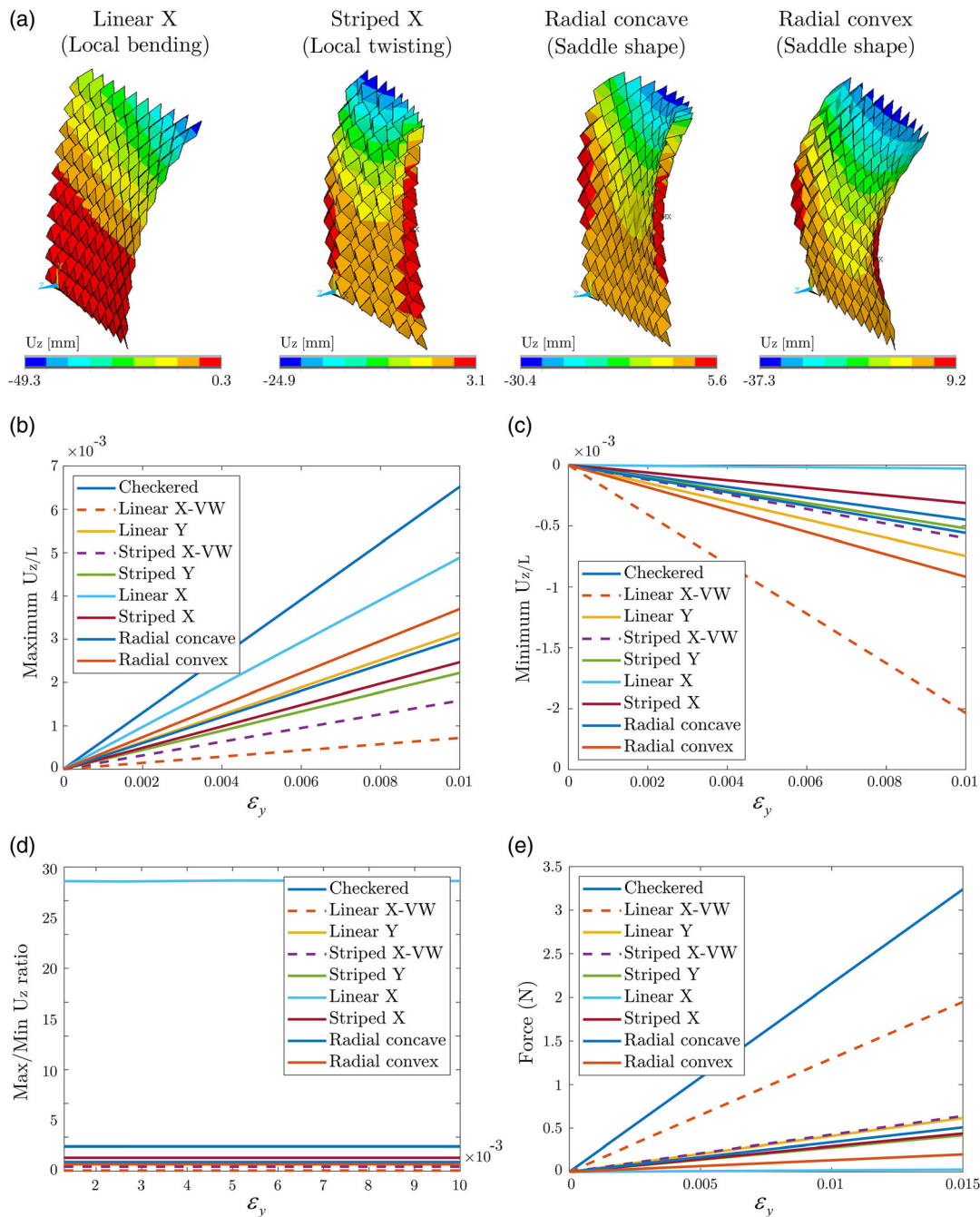


Figure 3. a) The curvatures resulting from Miura-ori origamis with linear X gradient, striped X, concave radial gradient, and convex radial gradient configurations. Variation of nondimensional b) maximum and c) minimum U_z with respect to ϵ_y . d) Variation of maximum/minimum U_z with respect to ϵ_y . e) Force–strain diagrams of all the origamis.

crease lines. One such combination based on zig-zag strips was introduced in ref. [21], and it was shown that such hybrid structures are flat-foldable.

Manipulation of Poisson's ratio, which was achieved by changing Miura-Ori characteristics spatially in this work, can be performed by other means to create similar 3D curvatures. As long as different regions of a flat plate are programmed to demonstrate different lateral behaviors upon receiving external

stimulus, the plate would demonstrate curvatures similar to what was proposed in this study. Examples include plates with nonuniform/gradient distribution of thermal expansion coefficient under heat stimulus, plates with nonuniform swelling factor distribution under adjustable environmental (humidity and/or chemical) conditions, and plates with nonuniform shape recovery coefficient under heat stimulus.^[22–24] In fact, the mechanical actuation technique proposed in this study

has the advantages of being inexpensive, easy to control, and mechanically durable.

As origamis are free from geometrical scales, the presented approaches can be generalized to other scales all the way from nano-scale to mega-structures. Therefore, these configurations can have applications in several engineering devices such as robotics,^[25] wearable devices (Figure 4a,b), self-folding assemblies,^[26] and self-morphing structures.^[27] Such applications are more realizable due to recent advances in manufacturing technologies such as additive manufacturing,^[19] stress within thin films,^[28] nano-lithography,^[29] and small-scale hinge constructions.^[30,31] The actuation can be performed either globally or locally. Locally, the actuation can be done by making regions at the sides of each unit cell inflatable or stretchable to create respectively pressure or contraction at the two ends of each cell. This actuation mechanism can be compared to auto-stress phenomenon in organs.^[32] Regardless of the actuation technique being local or global, each lattice structure deforms in such a way that it minimizes the total mechanical energy of the overall system.^[32] This can cause different bifurcations such as local buckling, single curvature, or double curvature depending on the unit cell distribution (see Figure 2 and 3).

The other fact to mention is that the proposed designs can also be used in hinged configurations. In fact, we tried constructing such hinged assemblies (Figure 4c). However, as the structures get larger and larger, and tessellation pattern numbers increase, the attention required to be paid to precision and accuracy increase exponentially. This is more pronounced in gradient assemblies. In case insufficient attention is paid to precision, very small inaccuracies in the placement of origami faces and attachment of the hinges can lead to very strong unwanted forces in sufficiently large structures. This not only decreases the robustness of the structure locally and globally but it also departs the structure from rigid foldability, which, in turn, introduces unwanted energy consumption through strain energy dissipation.

Finally, the basic gradient tessellations could be combined in dual or multiple configurations to give more complex shapes on demand. We have shown the benefits of such combinations in 2D gradient auxetic configurations for programming vase, barrel, and narrow-waisted shapes into the flat rectangular plates.^[17] Combinations of the designs proposed in this study can be implemented to develop deformable surfaces such as flexible yet strong clothing, soft robotics, deformable batteries,^[33,34]

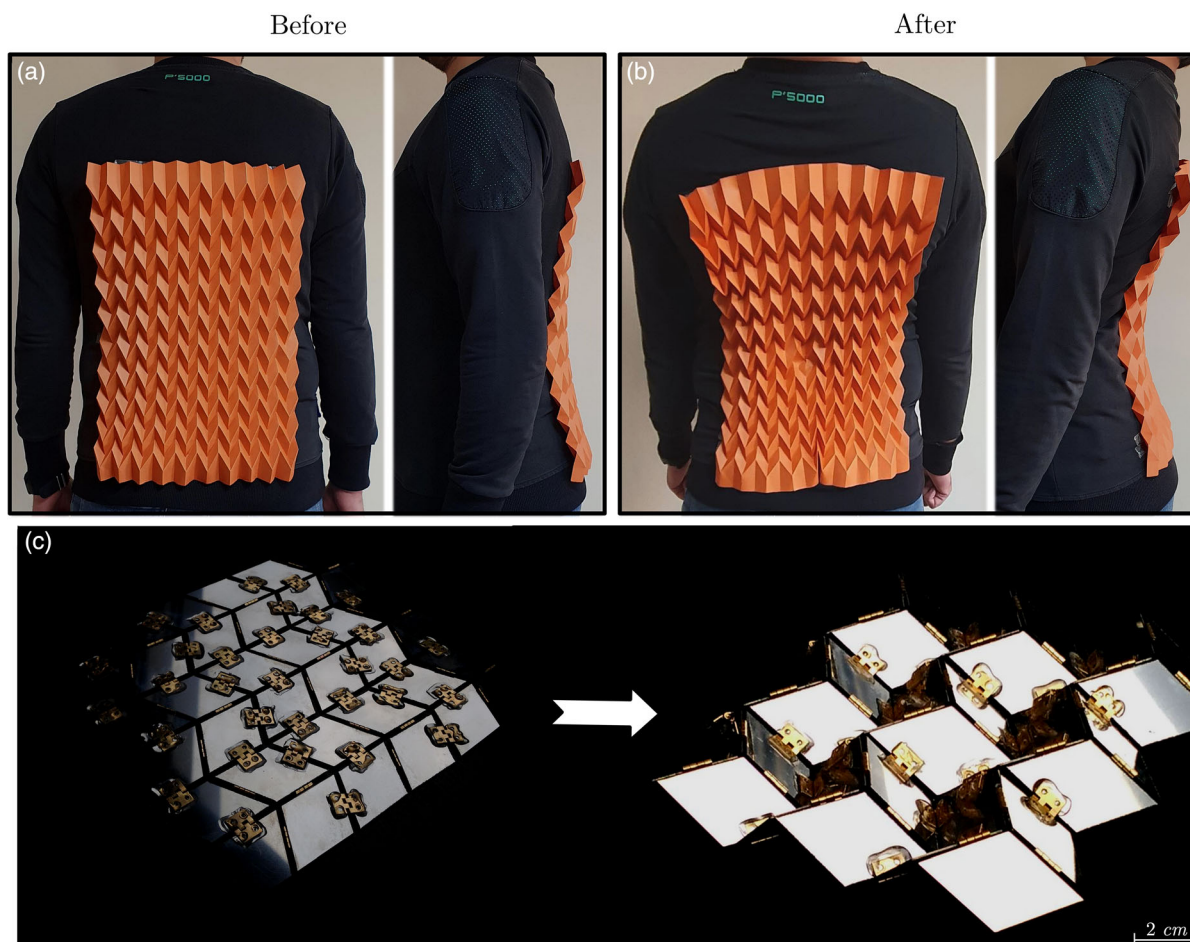


Figure 4. a,b) A demonstration of a potential application of linear-Y gradient origami lattice in wearable devices and shape-morphing clothing such as exosuits and diving dresses. The linear Y gradient origami tessellation takes a saddle shape similar to the curvature of human back when a person bends back. c) Hinged stainless steel Miura-ori origami tessellation before and after folding.

deformable electronics,^[35] and complex actuators.^[36] Origami-based deformable electronics could demonstrate the excellent performance of conventional rigid electrical components as well as high 3D deformability levels. The electronic performance in currently existing highly deformable thin-film-based solutions is usually diminished to a high degree due to low areal coverage.^[34]

6. Conclusions

In summary, gradient Miura-ori origamis were introduced as a method to create out-of-plane curvatures. Nine types of unit cell distributions in Miura-ori origami lattice structure such as checked, linear gradient, concave radial gradient, convex radial gradient, and striped were considered. These distributions of Miura-ori origami led to several out-of-plane 3D geometries with single- or double curvatures such as twisting, saddle, bending, local inflation, local twisting, local bending, and wavy shapes when the origami lattice structure was loaded in compression in the direction parallel to the origami mid-plane. All the Gaussian curvatures (negative, positive, and zero) were achieved using the proposed models. Our approach will help tailoring complex preprogrammed surface geometries by employing basic gradient distributions of Miura-ori origami as building blocks.

Conflict of Interest

The authors declare no conflict of interest.

Data Availability Statement

The data that support the findings of this study are available from the corresponding authors upon reasonable request.

Keywords

curvature, gradient, metamaterials, Miura-ori, origami

Received: December 19, 2022

Revised: January 27, 2023

Published online:

-
- [1] S. Kamrava, R. Ghosh, Z. Wang, A. Vaziri, *Adv. Eng. Mater.* **2019**, *21*, 1800895.
 [2] K. Mohammadi, M. Movahhedy, I. Shishkovsky, R. Hedayati, *Appl. Phys. Lett.* **2020**, *117*, 061901.
 [3] R. Hedayati, S. J. Salami, Y. Li, M. Sadighi, A. Zadpoor, *Phys. Rev. Appl.* **2019**, *11*, 034057.
 [4] E. Barchiesi, F. Di Cosmo, M. Laudato, in *Discrete and Continuum Models for Complex Metamaterials* (Eds: F. dell'Isola, D.J. Steigmann), Cambridge University Press, Cambridge, England **2020**.

- [5] R. Hedayati, A. Güven, S. Van Der Zwaag, *Appl. Phys. Lett.* **2021**, *118*, 141904.
 [6] N. Ghavidelnia, M. Bodaghi, R. Hedayati, *Materials* **2021**, *14*, 993.
 [7] C. Ai, Y. Chen, L. Xu, H. Li, C. Liu, F. Shang, Q. Xia, S. Zhang, *Adv. Eng. Mater.* **2021**, *23*, 2100473.
 [8] J. L. Silverberg, A. A. Evans, L. McLeod, R. C. Hayward, T. Hull, C. D. Santangelo, I. Cohen, *Science* **2014**, *345*, 647.
 [9] L. Mahadevan, S. Rica, *Science* **2005**, *307*, 1740.
 [10] A. E. Shyer, T. Tallinen, N. L. Nerurkar, Z. Wei, E. S. Gil, D. L. Kaplan, C. J. Tabin, L. Mahadevan, *Science* **2013**, *342*, 212.
 [11] L. H. Dudte, E. Vouga, T. Tachi, L. Mahadevan, *Nat. Mater.* **2016**, *15*, 583.
 [12] H. M. Kolken, A. Zadpoor, *RSC Adv.* **2017**, *7*, 5111.
 [13] K. Liu, T. Tachi, G. H. Paulino, *Nat. Commun.* **2019**, *10*, 4238.
 [14] Z. Y. Wei, Z. V. Guo, L. Dudte, H. Y. Liang, L. Mahadevan, *Phys. Rev. Lett.* **2013**, *110*, 215501.
 [15] H. Nassar, A. Lebé, L. Monasse, *Proc. R. Soc. A* **2017**, *473*, 20160705.
 [16] X. Dang, F. Feng, P. Plucinsky, R. D. James, H. Duan, J. Wang, arXiv preprint arXiv:2008.02349, **2020**.
 [17] R. Hedayati, M. Mirzaali, L. Vergani, A. Zadpoor, *APL Mater.* **2018**, *6*, 036101.
 [18] M. Schenk, S. D. Guest, *Proc. Natl. Acad. Sci.* **2013**, *110*, 3276.
 [19] J. Harris, G. McShane, *Int. J. Solids Struct.* **2020**, *185*, 448.
 [20] C. Lv, D. Krishnaraju, G. Konjevod, H. Yu, H. Jiang, *Sci. Rep.* **2014**, *4*, 5979.
 [21] M. Eidini, *Extreme Mech. Lett.* **2016**, *6*, 96.
 [22] M. Mehrpouya, A. Azizi, S. Janbaz, A. Gisario, *Adv. Eng. Mater.* **2020**, *22*, 2000296.
 [23] N. Roudbarian, M. Baniasadi, P. Nayyeri, M. Ansari, R. Hedayati, M. Baghani, *Smart Mater. Struct.* **2021**, *30*, 105006.
 [24] N. Roudbarian, E. Jebellat, S. Famouri, M. Baniasadi, R. Hedayati, M. Baghani, *Eur. J. Mech.-A: Solids* **2022**, *96*, 104676.
 [25] E. Hawkes, B. An, N. M. Benbernou, H. Tanaka, S. Kim, E. D. Demaine, D. Rus, R. J. Wood, *Proc. Natl. Acad. Sci.* **2010**, *107*, 12441.
 [26] S. Janbaz, R. Hedayati, A. Zadpoor, *Mater. Horiz.* **2016**, *3*, 536.
 [27] J. K. Paik, A. Byoungkwon, D. Rus, R. J. Wood, in *ICMC*, Venice, Italy **2012**.
 [28] V. B. Shenoy, D. H. Gracias, *MRS Bull.* **2012**, *37*, 847.
 [29] A. Matković, B. Vasić, J. Pešić, J. Prinz, I. Bald, A. R. Milosavljević, R. Gajić, *New J. Phys.* **2016**, *18*, 025016.
 [30] K. Kuribayashi, K. Tsuchiya, Z. You, D. Tomus, M. Umemoto, T. Ito, M. Sasaki, *Mater. Sci. Eng., A* **2006**, *419*, 131.
 [31] J. T. Overvelde, T. A. De Jong, Y. Shevchenko, S. A. Bercera, G. M. Whitesides, J. C. Weaver, C. Hoberman, K. Bertoldi, *Nat. Commun.* **2016**, *7*, 10929.
 [32] B. Moulia, *J. Plant Growth Regul.* **2000**, *19*, 19.
 [33] Y. Zhang, Y. Huang, J. A. Rogers, *Curr. Opin. Solid State Mater. Sci.* **2015**, *19*, 190.
 [34] Z. Song, T. Ma, R. Tang, Q. Cheng, X. Wang, D. Krishnaraju, R. Panat, C. K. Chan, H. Yu, H. Jiang, *Nat. Commun.* **2014**, *5*, 3140.
 [35] W. J. Song, S. Yoo, G. Song, S. Lee, M. Kong, J. Rim, U. Jeong, S. Park, *Batteries Supercaps* **2019**, *2*, 181.
 [36] R. V. Martinez, C. R. Fish, X. Chen, G. M. Whitesides, *Adv. Funct. Mater.* **2012**, *22*, 1376.